Phase diagrams of charged colloids from thermodynamic integration

2009 J. Phys.: Condens. Matter 21 465104

(http://iopscience.iop.org/0953-8984/21/46/465104)

J. Phys.: Condens. Matter **21** (2009) 465104 (7pp) doi:10.1088/0953-8984/21/46/465104

Phase diagrams of charged colloids from thermodynamic integration

A-P Hynninen[1] **and A Z Panagiotopoulos**[2]

Department of Chemical Engineering and Institute for the Science and Technology of Materials, Princeton University, Princeton, NJ 08544, USA

E-mail: azp@princeton.edu

Received 9 June 2009, in final form 17 September 2009
Published 26 October 2009
Online at stacks.iop.org/JPhysCM/21/465104

Abstract

We present full phase diagrams (including solid phases) of spherical charged colloids, using Monte Carlo sampling and thermodynamic integration of the Helmholtz free energy. Colloids and their co- and counterions are described by the primitive model for ionic systems that consists of hard-spheres with central point charges, while the solvent is taken into account solely through its dielectric constant. Two systems are considered: (i) a size-asymmetric system of oppositely charged spheres with size ratios $q = 0.3$ and 0.5 and (ii) a charge- and size-asymmetric system with colloid charge $Q = 10$ and counterions of charge -1 in the presence of monovalent added salt. In system (i), for both size ratios, the stable solid phase is equivalent to the NaCl crystal where the oppositely charged spheres take the lattice positions of Na and Cl ions. In system (ii), the phase diagram consists of gas–liquid and fluid–solid coexistence regions. We show that added salt stabilizes the fluid phase and shrinks the fluid–solid coexistence region, in agreement with experimental and theoretical results.

(Some figures in this article are in colour only in the electronic version)

1. Introduction

Charged colloidal suspensions consist of 10 nm–1 μm size macroions carrying between 10 and 10^4 electron charges that are suspended in a solvent (e.g. water) with co- and counterions. Due to electrostatic attractions between the colloids and the counterions, the counterions build a layer around the colloid called the double layer. In nature, colloids are found as globular proteins and micelles, but can also be synthesized as spheres and many other shapes. Colloids are of fundamental interest due to their importance in systems ranging from food and paper products to building blocks of novel photonic devices. One fascinating feature of charged colloids is the ability of same-charge objects to (effectively) attract each other. This phenomenon is called 'like-charge attraction' and its origin lies in the counterion–counterion correlations between the electric double layers [1–6]. Like-charge attraction is only present when the Coulomb interactions are strong in comparison to thermal fluctuations. This is typically not the case for colloids suspended in water with monovalent salt, for which interactions are weak because of the high dielectric constant of the medium. The condition of strong Coulomb interactions can be realized, however, in lower dielectric constant solvents or with multiply charged counterions. The systems of interest for the present study are strongly interacting and do not correspond to typical experimental systems in aqueous solutions. Examples of like-charge attraction include the reduced swelling of lyotropic liquid lamellar phases when monovalent ions are substituted by divalent ions [7, 8]. The very simplest computational model that reproduces like-charge attraction is the so-called primitive model in which the colloids and ions are represented as hard-spheres with charges at their centers and the solvent is taken into account as a continuum dielectric medium. Previous studies of the primitive model have showed that the system has a stable gas–liquid critical point and have determined its location for colloid charges $Q = 1$–10 times the counterion charge [9–14]. In earlier work [15], we have determined the full phase diagrams for salt-free charged colloids with point counterions. Results for colloid charge up to $Q = 50$ were obtained by thermodynamic

[1] Present address: National Renewable Energy Laboratory, Golden, CO 80401, USA.

[2] Author to whom any correspondence should be addressed.

integration and an approximate technique was developed for colloid charges up to $Q = 2000$.

In real charged colloidal suspensions, added salt consisting of co- and counterions is always present to some degree. There have been numerous theoretical [16–21] and experimental [22–24] studies of the effects of added salt on the phase behavior of charged colloids. Salt effects on phase diagrams have been studied by simulation primarily using effective, salt-mediated potentials for the colloid–colloid interactions [25–27]. In an earlier paper [13], the location of the gas–liquid critical point was determined as a function of the amount of added salt for an explicit-ion model colloid of charge $Q = 2$, 3, and 10. In this earlier work, the critical temperature and density were determined at a fixed chemical potential of added salt. While grand-canonical simulations can accurately locate the critical point, they cannot easily be used to determine phase coexistence between solid phases. In the present study, we address this issue by calculating the phase diagram using Helmholtz free energy methods, which accurately determine both gas–liquid and fluid–solid coexistence regions but are less accurate in determining vapor–liquid critical points. As an example, we calculate the phase diagram of a charge- and size-asymmetric primitive model colloidal system with charge $Q = 10$, at fixed temperature and varying chemical potential of added salt. For simplicity, we refer to this system as 'charge-asymmetric' in the rest of this paper. As another example of the use of this approach, we obtain the phase diagram of size-asymmetric charged spheres with opposite charges of equal magnitude and size ratios $q = 0.3$ and 0.5. This system is relevant for suspensions of oppositely charged nanoparticles or colloids [28–31].

The rest of this paper is organized as follows. In section 2, we present details of the thermodynamic integration approach used for calculations of the Helmholtz free energies. Section 3 presents our results for the solid–liquid and vapor–liquid transitions for the two systems studied. Section 4 concludes with a discussion of our findings and implications for future studies of full phase diagrams of charged colloids.

2. Methods

We performed MC simulations in cubic simulation boxes within periodic boundary conditions. Particles interact via the Coulomb potential plus hard-core repulsion given by

$$\frac{u(r_{ij})}{k_{\mathrm{B}}T} = \begin{cases} \dfrac{q_i q_j \sigma}{T^* r_{ij}} & \text{if } r_{ij} \geqslant \frac{1}{2}(\sigma_i + \sigma_j) \\ \infty & \text{if } r_{ij} < \frac{1}{2}(\sigma_i + \sigma_j), \end{cases} \tag{1}$$

where q_i and q_j are the charges of particles i and j, r_{ij} is the distance between the particles, $T^* = \sigma/\lambda_{\mathrm{B}}$ is a reduced temperature, σ is the diameter of the colloids, $\lambda_{\mathrm{B}} = e^2/\epsilon k_{\mathrm{B}}T$ is the Bjerrum length of the solvent, k_{B} the Boltzmann constant, and T the absolute temperature. The long-ranged Coulomb interactions were calculated using the Ewald summation method [32] with 514 reciprocal space vectors and conducting boundary conditions. Density was measured using the packing fraction η, defined as the fraction of volume V taken up by the colloids and the ions. For the charge-asymmetric system the packing fraction is

$$\eta = \frac{\pi}{6}\frac{N_{\mathrm{col}}\sigma^3 + N_{\mathrm{ion}}\sigma_{\mathrm{ion}}^3}{V}, \tag{2}$$

where N_{col} and N_{ion} are the number of colloids and ions. For the size-asymmetric system, the packing fraction becomes

$$\eta = \frac{\pi}{6}(1+q^3)\sigma^3\frac{N_{\mathrm{col}}}{V}, \tag{3}$$

where N_{col} is the number of large and small spheres and q is the size ratio. The MC displacement moves for colloids were accelerated using cluster moves [33, 34].

For both the size- and charge-asymmetric systems, the Helmholtz free energy $F(N_{\mathrm{col}}, N_{\mathrm{small}}, V, T)$ was obtained from thermodynamic integration. N_{small} is the number of small particles: $N_{\mathrm{small}} = QN_{\mathrm{col}} + 2\langle N_{\mathrm{salt}}\rangle$ in the case of charge-asymmetric case and $N_{\mathrm{small}} = N_{\mathrm{col}}$ in the size-asymmetric case. For the charge-asymmetric system, the average number of salt pairs $\langle N_{\mathrm{salt}}\rangle$ is calculated using semi-grand-canonical simulations where the salt chemical potential μ_{salt}, the number of colloids, volume, and the temperature are fixed. The resulting phase diagram is presented in the chemical potential of salt μ_{salt}, packing fraction η plane at constant temperature T^*. In the thermodynamic integration method, the free energy is calculated as the difference between a reference system (whose free energy is known) and the actual system of interest. The total Helmholtz free energy is then given as the sum of the reference system free energy and the free energy difference. For the fluid phase, the thermodynamic integration method is also known as Kirkwood's coupling parameter method [32, 35]. In this method, an auxiliary potential energy function is introduced,

$$U_\lambda(\mathbf{r}^N) = U_{\mathrm{HS}}(\mathbf{r}^N) + \lambda U(\mathbf{r}^N), \tag{4}$$

where $\lambda \in [0, 1]$ is a coupling parameter and N is the total number of particles in the system: $N = (Q+1)N_{\mathrm{col}} + 2\langle N_{\mathrm{salt}}\rangle$ in the charge-asymmetric case and $N = 2N_{\mathrm{col}}$ in the size-asymmetric case. In equation (4), at $\lambda = 1$, we recover the system of interest, while at $\lambda = 0$, the system reduces to the reference state. The Helmholtz free energy is given by

$$F(N, V, T) = F_{\mathrm{HS}}(N_{\mathrm{col}}, N_{\mathrm{small}}, V, T) + \int_0^1 \left\langle U(\mathbf{r}^N)\right\rangle_\lambda \, \mathrm{d}\lambda, \tag{5}$$

where F_{HS} is the free energy of the reference state. For the fluid phase, this is a mixture of N_{col} large hard-spheres and N_{small} small hard-spheres and can be computed using the analytical formula from [36]. The integral in equation (5) is evaluated numerically using the Gauss–Legendre quadrature [37] where

$$\int_0^1 \left\langle U(\mathbf{r}^N)\right\rangle_\lambda \, \mathrm{d}\lambda \approx \tfrac{1}{2}\sum_{i=1}^{m} w_i \left\langle U(\mathbf{r}^N)\right\rangle_{\lambda_i}. \tag{6}$$

In equation (6), the ensemble averages are calculated at coupling parameter values $\lambda_i = \frac{1}{2}(x_i + 1)$, where x_i is the ith root of the Legendre polynomial $P_m(x)$ and the weights

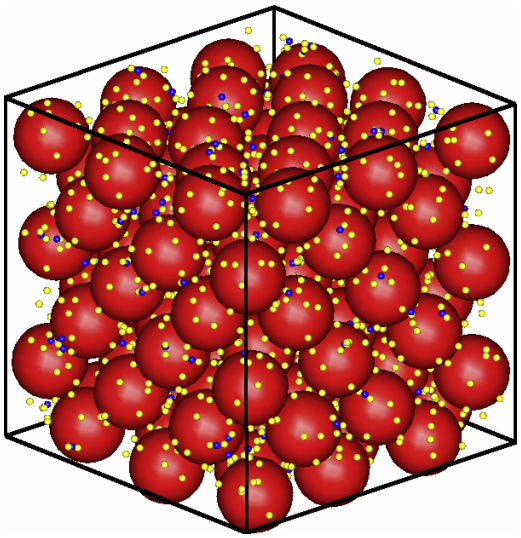

Figure 1. A snapshot of the fcc crystal structure in the charge-asymmetric system at $\mu_{\text{salt}} = -8k_{\text{B}}T$ and $\eta = 0.5$. In this snapshot $N_{\text{col}} = 108$ and $N_{\text{salt}} = 146$. The large (red) spheres represent the colloids with charge $Q = 10$ and the small dark (blue) and light (yellow) spheres represent the co- and counterions with charges $+1$ and -1, respectively.

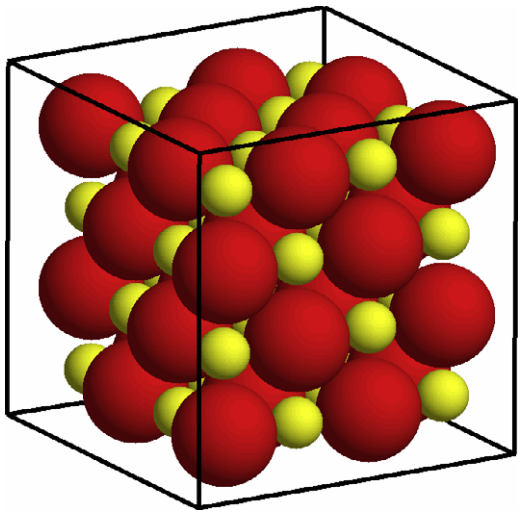

Figure 2. A snapshot of the NaCl crystal structure in the size-asymmetric system with opposite charges of equal magnitude and size ratio $q = 0.5$. In this snapshot $N_{\text{col}} = N_{\text{small}} = 32$.

are given by $w_i = \frac{2}{1-x_i^2}[P'_m(x_i)]^2$. For the solid phase of the charge-asymmetric system, the reference state in equation (5) is a face-centered-cubic (fcc) solid of large hard-spheres (colloids) mixed with a fluid of small hard-spheres (the co- and counterions), see figure 1. Figure 1 shows a snapshot of a fcc crystal at $\mu_{\text{salt}} = -8k_{\text{B}}T$ and $\eta = 0.5$, where the large (red) spheres are the colloids and the small dark (blue) and light (yellow) spheres are the co- and counterions, respectively.

The free energy of the reference state is calculated from

$$F_{\text{HS}}(N_{\text{col}}, N_{\text{ion}}, V, T) = F_{\text{HS}}(N_{\text{col}}, 0, V, T) + \int_0^{N_{\text{ion}}} \langle \mu_{\text{ion}}(N_{\text{col}}, n, V, T) \rangle \, \mathrm{d}n, \quad (7)$$

where $F_{\text{HS}}(N_{\text{col}}, 0, V, T)$ is the free energy of a hard-sphere fcc crystal [38] and $\langle \mu_{\text{ion}}(N_{\text{col}}, n, V, T) \rangle$ is the ensemble average of the chemical potential of small hard-spheres. In practice, to evaluate the integral in equation (7), we calculate the chemical potential $\langle \mu_{\text{ion}}(N_{\text{col}}, n, V, T) \rangle$ between every 25 (or 50) ion numbers n using the Widom insertion method [32, 39], perform a Padé approximation on the data in order to obtain a smooth function, and finally numerically integrate the Padé approximation.

The crystal structure in the size-asymmetric systems is equivalent to the NaCl crystal where the positive and negative spheres take the lattice positions of the Na and Cl ions. Figure 2 shows a snapshot of the NaCl crystal structure for $q = 0.5$. The thermodynamic integration method given in equation (5) works only for crystal structures with a stable hard-sphere reference state (at $\lambda = 0$). In practice then, the method is limited to fcc and hexagonal-close-packed (hcp) crystals at packing fractions above the hard-sphere melting packing fraction $\eta \approx 0.548$ [40]. In particular, the method cannot be used to calculate the free energy of the NaCl crystal since the simple cubic solid is unstable for hard-spheres. Fortunately, in all these other cases, the Helmholtz free energy can still be calculated by simply changing the reference state from hard-spheres to an Einstein crystal where the particles are tied to their ideal lattice positions by harmonic springs. This method was first presented by Frenkel and Ladd for calculating the free energy of hard-spheres [41] and has since been refined and applied to many other systems [32, 42]. For the charge-asymmetric system, one starts from an Einstein crystal where the particles are tied to their ideal lattice positions by harmonic springs. Step by step, the springs are removed and one recovers the original interactions. The auxiliary potential energy function that includes the harmonic springs is given by

$$U_\lambda(\mathbf{r}^N) = U_{\text{HS}}(\mathbf{r}^N) + (1-\lambda)U(\mathbf{r}^N) + k_{\text{B}}T\lambda\alpha \sum_{i=1}^{N_{\text{col}}} (\mathbf{r}_i - \mathbf{r}_{0,i})^2/\sigma^2. \quad (8)$$

In equation (8), the potential energy term $U(\mathbf{r}^N)$ vanishes at $\lambda = 1$ and the system interacts via a hard-core potential $U_{\text{HS}}(\mathbf{r}^N)$ plus harmonic springs. The Helmholtz free energy is now obtained from

$$F(N, V, T) = F_{\text{Ein}}(N_{\text{col}}, N_{\text{ion}}, V, T, \alpha) - \int_0^1 \mathrm{d}\lambda \left\langle k_{\text{B}}T\alpha \sum_{i=1}^{N_{\text{col}}} (\mathbf{r}_i - \mathbf{r}_{0,i})^2/\sigma^2 - U(\mathbf{r}^N) \right\rangle_\lambda^{\text{CM}}, \quad (9)$$

where the free energy of the Einstein crystal is given by

$$F_{\text{Ein}}(N_{\text{col}}, N_{\text{ion}}, V, T, \alpha) = \frac{3(N_{\text{col}}-1)}{2} k_{\text{B}}T \ln\left(\frac{\alpha}{\pi}\right) + k_{\text{B}}T \ln\left(\frac{\sigma^3}{V N_{\text{col}}^{1/2}}\right) - 6\ln[1 - P(\alpha, \eta)] + \int_0^{N_{\text{ion}}} \langle \mu_{\text{ion}}(N_{\text{col}}, n, V, T) \rangle \, \mathrm{d}n, \quad (10)$$

where

$$P(\alpha,\eta) = \frac{\mathrm{erf}\left[\sqrt{\alpha/2}(\sigma+a)\right] + \left[\sqrt{\alpha/2}(\sigma-a)\right]}{2} - \frac{\exp\left[-\alpha(\sigma-a)^2/2\right] - \exp\left[-\alpha(\sigma+a)^2/2\right]}{a\sqrt{2\pi\alpha}}, \quad (11)$$

is the probability that two nearest neighbors overlap in a fcc crystal. In equation (10), the first term is the free energy of the Einstein crystal with a fixed center of mass, and the second term is a correction term for the fixed center of mass. The third term is a correction term that takes into account configurations where nearest neighbors overlap. The fourth term in equation (10) is the free energy change due to adding the N_{ion} small hard-spheres (the microions) into an Einstein crystal of N_{col} large hard-spheres (the colloids) with coupling parameter α. This term is calculated in the similar way as in equation (7). In equation (9), the ensemble average $\langle\cdots\rangle_\lambda^{\mathrm{CM}}$ is calculated with a Boltzmann factor $\exp(-U_\lambda/k_{\mathrm{B}}T)$ for a crystal with a fixed center of mass. The integral in equation (9) is evaluated numerically using the Gauss–Legendre method given by equation (6).

In the size-asymmetric case the auxiliary potential energy function is given by

$$U_\lambda(\mathbf{r}^N) = U_{\mathrm{HS}}(\mathbf{r}^N) + U(\mathbf{r}^N) + k_{\mathrm{B}}T\lambda\alpha\sum_{i=1}^{N}(\mathbf{r}_i - \mathbf{r}_{0,i})^2/\sigma^2. \quad (12)$$

Note that the difference between equations (8) and (12) is that equation (12) retains the Coulomb interactions at $\lambda = 0$. In equation (12), the reference state at $\lambda = 1$ is a non-interacting Einstein crystal where the spring constants are chosen so large that the neighboring spheres do not overlap. Therefore the overlap probability $P(\alpha,\eta) = 0$ and the system behaves as a harmonic crystal with mean-square displacement given by

$$\langle r^2\rangle_{\lambda=1} = \langle r^2\rangle_{\mathrm{Einst}} = \frac{3(N-1)}{2N\alpha}. \quad (13)$$

At $\lambda = 1$, the particles are vibrating harmonically about their minimum energy lattice positions determined by the Coulombic potential energy. The reference state free energy is then given by the free energy of an Einstein crystal plus the Coulomb potential energy of an ideal NaCl crystal, i.e., the Madelung energy. The Helmholtz free energy is now obtained from

$$F(N,V,T) = U(\mathbf{r}_0^N) + F_{\mathrm{Ein}}(N,V,T,\alpha) - \int_0^1 \mathrm{d}\lambda\left\langle k_{\mathrm{B}}T\alpha\sum_{i=1}^{N}(\mathbf{r}_i - \mathbf{r}_{0,i})^2/\sigma^2\right\rangle_\lambda^{\mathrm{CM}}, \quad (14)$$

where $U(\mathbf{r}_0^N)$ is the Madelung energy and

$$F_{\mathrm{Ein}}(N,V,T,\alpha) = \frac{3(N-1)}{2}k_{\mathrm{B}}T\ln\left(\frac{\alpha}{\pi}\right) + k_{\mathrm{B}}T\ln\left(\frac{\sigma^3}{VN^{1/2}}\right). \quad (15)$$

In order to make the numerical integration in equation (14) more accurate, we re-parameterize the integration variable to obtain a more smoothly varying integrand. To this end, we employ the scheme introduced in [32, 41], where the integrand is re-written as

$$\int_{\ln c}^{\ln(\alpha+c)}(c+\alpha\lambda)\left\langle\sum_{i=1}^{N}(\mathbf{r}_i - \mathbf{r}_{0,i})^2/\sigma^2\right\rangle_\lambda^{\mathrm{CM}}\mathrm{d}[\ln(c+\alpha\lambda)], \quad (16)$$

where

$$c = \frac{1}{\left\langle\sum_{i=1}^{N}(\mathbf{r}_i - \mathbf{r}_{0,i})^2/\sigma^2\right\rangle_0^{\mathrm{CM}}}. \quad (17)$$

In using this re-parameterization, one first calculates the mean-square displacement at $\lambda = 0$ to obtain an estimate for c. One can easily check that the integrand in equation (16) varies between 1.0 at $\lambda = 0$ and approximately 1.5 at $\lambda = 1$ (because $N \gg 1$ and $\alpha \gg c$). These analytical limits serve as an easy check for making sure the method is working correctly. In particular, if the integrand does not converge to 1.0 at $\lambda = 0$, it is likely that the solid has melted or reconfigured to another crystal structure.

For the charge-asymmetric case, we also tried to calculate free energies by starting from a salt-free system and integrating the salt equation of state (N_{salt}, μ_{salt}). In this case, the equation of state is obtained from canonical MC simulation using the Widom insertion method. However, this approach failed because the equation of state data was too noisy. The likely reason for the noisiness is the high electrostatic coupling in the system: counterions are preferentially placed around the colloids but such optimal placement happens only rarely in the uniform random insertions used in the Widom method. This makes gathering good statistics difficult. Note that the same problem is not present in the uncharged system and therefore the evaluation of the integrals in equations (7) and (10) is feasible. Additionally, in this case, the hard-sphere simulations are much faster since there is no need for Ewald summation.

3. Results

The charge-asymmetric simulations were performed with $N_{\mathrm{col}} = 108$ colloids. A typical simulation run consisted of 10 000 equilibration and 40 000 production MC steps (trials to displace each particle once). The CPU time of a single MC run varied from 3 h at low salt concentration to 6 h at high salt concentration on 2.6 GHz Intel processors. Since we used 10 integration points for evaluating the integrals in equations (5) and (9), this adds up to 30–60 CPU hours for each Helmholtz free energy point and 438 days of CPU time for the entire phase diagram. Therefore, although the majority of the computational effort can be run in parallel, constructing the phase diagram takes up a lot of computational resources. This is why we calculated the charge-asymmetric phase diagram only for a single temperature. Most of the size-asymmetric simulations were performed for system size $N = 64$, but we also used simulations with $N = 108$ and 216 to check for finite size effects. Again, the simulations consisted of 10 000 equilibration and 40 000 production steps. The effect of the system size was determined to be smaller than other sources of error.

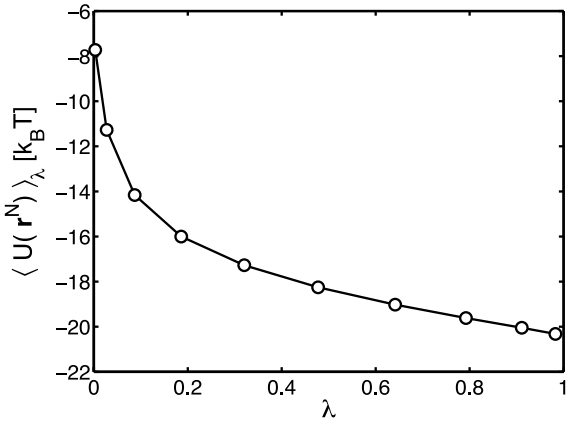

Figure 3. The integrand in equation (5) as a function of the integration variable λ for a fluid phase at $\eta = 0.17$ and $T^* = 0.044$.

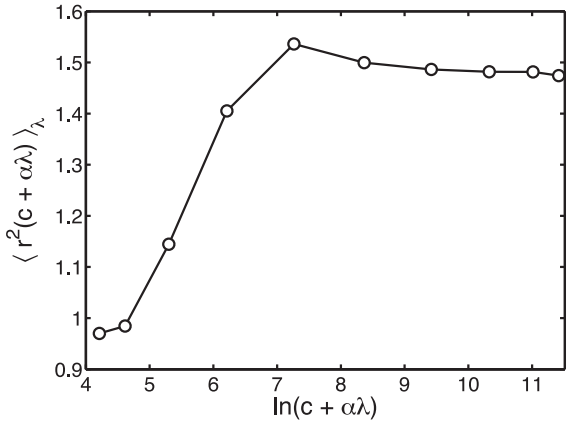

Figure 4. The integrand in equation (16) of the size-asymmetric system with $q = 0.5$ as a function of the integration variable $\ln(c + \alpha\lambda)$ for a (NaCl) solid phase at $\eta = 0.51$ and $T^* = 0.044$.

Figure 3 shows the integrand in equation (5) for the size-asymmetric system with opposite charges of equal magnitude and $q = 0.5$ as a function of the integration variable λ for a fluid phase at $\eta = 0.17$ and $T^* = 0.044$. The integrand is evaluated at 10 integration points that are distributed using the Gauss–Legendre scheme. We tested the accuracy of the numerical integration by increasing the number of integration points to 20 and the result was the same within the error estimate. Figure 4 shows the integrand in equation (16) of the size-asymmetric system with $q = 0.5$ as a function of the integration variable $\ln(c + \alpha\lambda)$ for a (NaCl) solid phase at $\eta = 0.51$ and $T^* = 0.044$. We see from figure 4 that the integrand varies between 1.0 at $\lambda = 0$ and approximately 1.5 at $\lambda = 1$, as was discussed in section 2. Figure 5 shows the Helmholtz free energy per volume as a function of packing fraction for the size-asymmetric system with $q = 0.5$ and $T^* = 0.06$. We have subtracted a linear function to highlight the phase coexistence between a gas phase at $\eta = 0.006$ and a liquid phase at $\eta = 0.14$, which can be seen using a common tangent construction. Figure 6 plots the Helmholtz free energy of the same system at $T^* = 0.044$ and shows a phase coexistence between a fluid at $\eta = 0.38$ and a solid

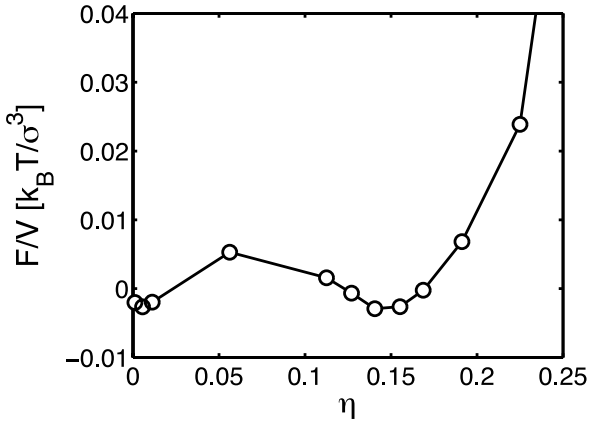

Figure 5. Helmholtz free energy per volume F/V as a function of packing fraction η for the size-asymmetric system with $q = 0.5$ and $T^* = 0.06$. The data shows a phase coexistence between a gas phase at $\eta = 0.006$ and a liquid phase at $\eta = 0.14$.

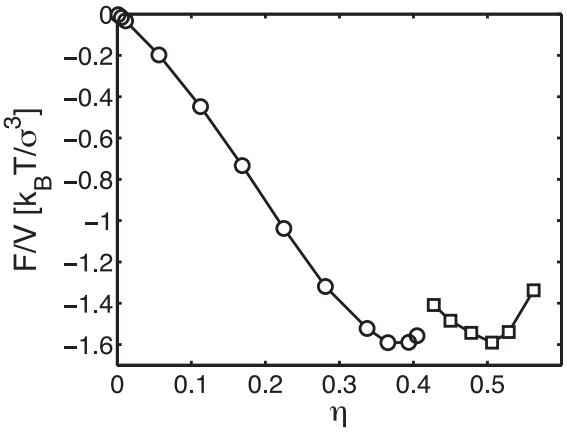

Figure 6. Helmholtz free energy per volume F/V as a function of packing fraction η for the size-asymmetric system with $q = 0.5$ and $T^* = 0.044$. The data shows a phase coexistence between a fluid phase at $\eta = 0.38$ and a solid phase at $\eta = 0.51$.

phase at $\eta = 0.51$. These plots were used to construct the phase diagrams shown in figures 7 and 8 for size ratios $q = 0.3$ and $q = 0.5$, respectively, in the packing fraction η, reduced temperature T^* representation. The shaded areas denote phase coexistence regions between gas and liquid, and fluid and NaCl solid. The tie lines in the coexistence regions are horizontal and the symbols mark the location where the calculations were performed. The stars denote the critical points and the solid (red) lines denote the gas–liquid phase coexistence lines determined using grand-canonical MC simulations. The details of the grand-canonical simulations can be found in [12–14, 43]. As can be seen, the grand-canonical results agree well with the Helmholtz free energy results, giving us confidence in the methods presented in this paper. The two phase diagrams for the size-asymmetric systems share common features with the corresponding phase diagram for the restricted primitive model for electrolytes (RPM) [30, 44], which corresponds to $q = 1$. Because of the size asymmetry, however, the fluid crystallizes into a solid with the NaCl structure, rather than

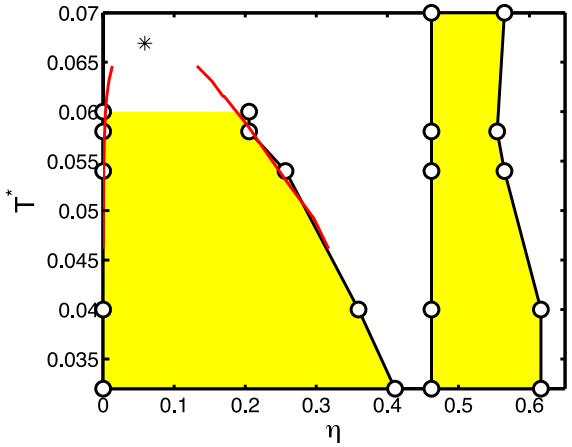

Figure 7. Phase diagram of primitive model charged spheres with opposite charges of equal magnitude and size ratio $q = 0.3$ in the packing fraction η, reduced temperature T^* representation. The shaded regions marks phase coexistence where tie lines are horizontal. Estimated uncertainties are comparable to symbol size.

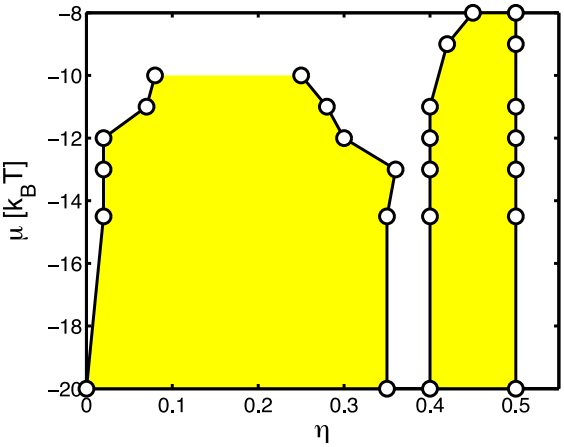

Figure 9. Phase diagram of primitive model charged colloids with charge $Q = 10$ and added monovalent salt in the packing fraction η, salt chemical potential μ_{salt} representation at reduced temperature $T^* = 0.56$. The shaded regions marks phase coexistence where tie lines are horizontal. Estimated uncertainties are comparable to symbol size.

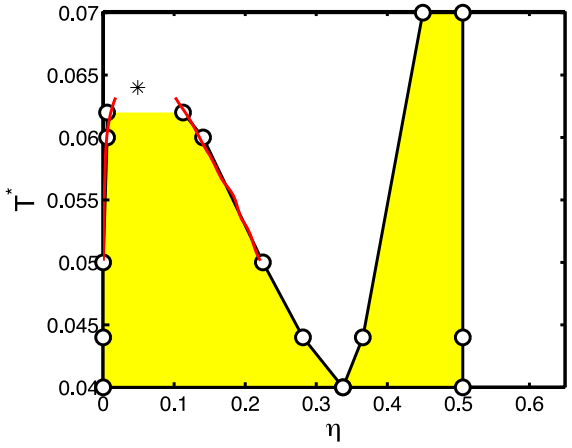

Figure 8. Phase diagram of primitive model charged spheres with opposite charges of equal magnitude and size ratio $q = 0.5$ in the packing fraction η, reduced temperature T^* representation. The shaded regions marks phase coexistence where tie lines are horizontal. Estimated uncertainties are comparable to symbol size.

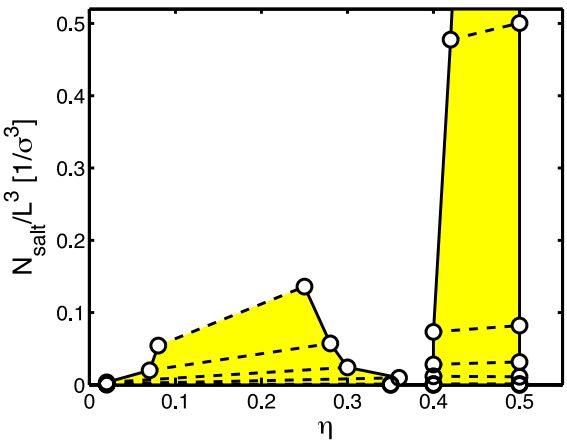

Figure 10. Phase diagram of primitive model charged colloids with charge $Q = 10$ and added monovalent salt in the packing fraction η, salt concentration N_{salt}/L^3 representation at reduced temperature $T^* = 0.56$. The shaded regions marks phase coexistence and the dashed lines denote tie lines between coexisting phases. Estimated uncertainties are comparable to symbol size.

the CsCl structure into which the RPM liquid crystallizes at temperatures comparable to the gas–liquid critical temperature.

Figure 9 shows the phase diagram of the charge-asymmetric system with colloids of charge $Q = 10$ and monovalent added salt (i.e., co- and counterions with charges $+1$ and -1, respectively) in the packing fraction η, salt chemical potential μ_{salt} representation at reduced temperature $T^* = 0.56$. In figure 9, the lowest salt chemical potential $\mu_{\text{salt}} = -20k_{\text{B}}T$ is equivalent to the case of no added salt (i.e. $\mu_{\text{salt}} = -\infty$) and the highest salt concentration is at $\mu_{\text{salt}} = -8k_{\text{B}}T$. Figure 10 shows the same phase diagram in the packing fraction η, salt concentration N_{salt}/L^3 representation. In figure 10, the dashed lines denote tie lines between coexisting phases and the highest salt concentration points shown correspond to salt chemical potential $\mu_{\text{salt}} = -9k_{\text{B}}T$. The size of the microions was set to $\sigma_{\text{ion}} = 0.1\sigma$, which is small enough so that the salt-free ($\mu_{\text{salt}} = -20k_{\text{B}}T$) results agree with point-like ion results [15] but at the same time large enough so that the salt component itself does not undergo gas–liquid phase separation. The shaded areas denote phase coexistence regions between gas and liquid, and fluid and fcc solid. The tie lines in the coexistence regions are horizontal. As can be seen from figure 9, the phase diagram has the familiar gas–liquid and fluid–solid coexistence regions. Gas–liquid phase coexistence terminates at a critical point around $\mu_{\text{salt}} \approx -11k_{\text{B}}T$. Note that the methods employed here do not allow for an accurate determination of the critical point. Figure 9 shows that the fluid–solid coexistence region becomes narrower with increasing salt, as seen experimentally [22] and in theoretical studies of Yakawa systems [17, 19]. The phase diagram is again qualitatively similar to that for the restricted primitive model for electrolytes (RPM) [30, 44], with the

temperature for the RPM being analogous to salt concentration for the system with added salt. The solid–fluid transition cannot be determined at higher salt chemical potentials in the present study because of computational time limitations.

The other stable crystal structure for charged colloids is the body-centered-cubic (bcc) solid. From our earlier work [15], we know that bcc is not stable at zero added salt (where $\mu_{\text{salt}} = -20k_{\text{B}}T$). Since adding salt makes the effective colloid–colloid interactions less attractive and ultimately repulsive, it is possible that the bcc phase could be stable at high salt chemical potentials around $\mu_{\text{salt}} = -8k_{\text{B}}T$, however, in the current paper we have not studied this possibility further.

4. Conclusions

We have applied Helmholtz free energy thermodynamic integration methods to obtain the phase diagram of charged colloids. The calculations were performed within the primitive model using Monte Carlo simulations. Two systems were considered: (i) a size-asymmetric system that consists of equal amounts of oppositely charged spheres with size ratios $q = 0.3$ and 0.5, and (ii) a charge- and size-asymmetric system with colloid charge $Q = 10$ in the presence of monovalent added salt (i.e., co- and counterions with charges $+1$ and -1, respectively). For the size-asymmetric system, we calculated the phase diagram in the packing fraction η, reduced temperature T^* plane. The phase diagram consists of gas, liquid, and solid phases, and their coexistence regions. The stable solid phase is analogous to the NaCl crystal where the oppositely charged spheres take the lattice positions of Na and Cl ions. In the case of charge-asymmetric colloids, we have calculated the full phase diagram of charged colloids with charge $Q = 10$ times the counterion charge in the presence of monovalent added salt. The phase diagram is presented for fixed reduced temperature T^* in the packing fraction η, chemical potential of added salt μ_{salt} plane, and consists of gas, liquid, and solid phases, and phase coexistence regions. The stable solid phase is an fcc crystal of large spheres (colloids). With increasing added salt, the gas–liquid coexistence shrinks and terminates in a critical point, stabilizing the fluid phase. The stabilization of the fluid phase with added salt has been observed experimentally in [22]. The fluid–solid coexistence region also shrinks with increasing added salt.

The computational methods used in this work can be applied in principle to any charged colloidal system, with or without added salt. However, sampling difficulties are expected for very high charge asymmetries in the presence of salt. Also, an exhaustive investigation of alternative crystal structures needs to be performed to determine the stable solid phase in the size-asymmetric system.

Acknowledgments

This publication is based on work supported by the Princeton Center for Complex Materials, a National Science Foundation MRSEC (Award DMR-0819860) and the Department of Energy, Office of Basic Energy Sciences (DE-FG02-09ER16057).

References

[1] Linse P and Lobaskin V 1999 *Phys. Rev. Lett.* **83** 4208
[2] Levin Y 2002 *Rep. Prog. Phys.* **65** 1577–632
[3] Linse P 2002 *J. Phys.: Condens. Matter* **14** 13449
[4] Allahyarov E, Zaccarelli E, Sciortino F, Tartaglia P and Lowen H 2007 *Europhys. Lett.* **78** 38002
[5] Hynninen A P and Panagiotopoulos A Z 2008 *Mol. Phys.* **106** 2039–51
[6] Brulkhno A V, Akesson T and Jönsson B 2009 *J. Phys. Chem.* B **113** 6766
[7] Khan A, Fontell A and Lindman B 1984 *J. Colloid Interface Sci.* **101** 193
[8] Kang C and Khan A 1993 *J. Colloid Interface Sci.* **156** 218
[9] Yan Q and de Pablo J J 2001 *Phys. Rev. Lett.* **86** 2054
[10] Rescic J and Linse P 2001 *J. Chem. Phys.* **114** 10131–6
[11] Yan Q and de Pablo J J 2002 *Phys. Rev. Lett.* **88** 095504
[12] Panagiotopoulos A Z and Fisher M E 2002 *Phys. Rev. Lett.* **88** 045701
[13] Hynninen A P, Dijkstra M and Panagiotopoulos A Z 2005 *J. Chem. Phys.* **123** 084903
[14] Cheong D W and Panagiotopoulos A Z 2003 *J. Chem. Phys.* **119** 8526
[15] Hynninen A P and Panagiotopoulos A Z 2007 *Phys. Rev. Lett.* **98** 198301
[16] van Roij R, Dijkstra M and Hansen J P 1999 *Phys. Rev.* E **59** 2010–25
[17] Hynninen A P and Dijkstra M 2003 *Phys. Rev.* E **68** 021407
[18] Zoetekouw B and van Roij R 2006 *Phys. Rev. Lett.* **97** 258302
[19] Denton A R 2006 *Phys. Rev.* E **73** 041407
[20] Warren P B 2006 *Phys. Rev.* E **73** 011411
[21] Denton A R 2007 *Phys. Rev.* E **76** 051401
[22] Sirota E B, Ouyang H D, Sinha S K, Chaikin P M, Axe J D and Fujii Y 1989 *Phys. Rev. Lett.* **62** 1524–7
[23] Reus V, Belloni L, Zemb T, Lutterbach N and Versmold H 1997 *J. Physique* II **7** 603–26
[24] Yethiraj A and van Blaaderen A 2003 *Nature* **421** 513–7
[25] Robbins M O, Kremer K and Grest G S 1988 *J. Chem. Phys.* **88** 3286–312
[26] Hamaguchi S, Farouki R T and Dubin D H E 1997 *Phys. Rev.* E **56** 4671–82
[27] Lu B and Denton A R 2007 *Phys. Rev.* E **75** 061403
[28] Leunissen M E, Christova C G, Hynninen A P, Royall C P, Campbell A I, Imhof A, Dijkstra M, van Roij R and van Blaaderen A 2005 *Nature* **437** 235
[29] Bartlett P and Campbell A I 2005 *Phys. Rev. Lett.* **95** 128302
[30] Hynninen A P, Leunissen M E, van Blaaderen A and Dijkstra M 2006 *Phys. Rev. Lett.* **96** 018303
[31] Hynninen A P, Christova C G, van Roij R, van Blaaderen A and Dijkstra M 2006 *Phys. Rev. Lett.* **96** 138308
[32] Frenkel D and Smit B 2002 *Understanding Molecular Simulations* 2nd edn (New York: Academic)
[33] Lobaskin V and Linse P 1999 *J. Chem. Phys.* **111** 4300
[34] Linse P 2005 *Adv. Polym. Sci.* **185** 111
[35] Kirkwood J G 1935 *J. Chem. Phys.* **3** 300
[36] Mansoori G A, Carnahan N F, Starling K E and Leland T W Jr 1971 *J. Chem. Phys.* **54** 1523
[37] Abramowitz M and Stegun I 1970 *Handbook of Mathematical Functions* (New York: Dover)
[38] Speedy R J 1998 *J. Phys.: Condens. Matter* **10** 4387
[39] Widom B 1963 *J. Chem. Phys.* **39** 2802
[40] Hoover W G and Ree F H 1968 *J. Chem. Phys.* **49** 3609
[41] Frenkel D and Ladd A J C 1984 *J. Chem. Phys.* **81** 3188
[42] Polson J M, Trizac E, Pronk S and Frenkel D 2000 *J. Chem. Phys.* **112** 5339
[43] Romero-Enrique J, Orkoulas G, Panagiotopoulos A Z and Fisher M E 2000 *Phys. Rev. Lett.* **85** 4558
[44] Vega C, Abascal J L F, McBride C and Bresme F 2003 *J. Chem. Phys.* **119** 964